DOI: 10.24352/UB.OVGU-2019-003 TECHNISCHE MECHANIK, 39, 1, (2019), 16 - 29
submitted: September 4, 2018

Planar Elongation Flow Analysis of Non-Newtonian Fluids Using a Disk-Shaped Bob

S. Ito, S. Iwata, Y. Sugihara, T. Takahashi

Planar elongation viscosity is a material property involved in extensional deformation, which plays a significant role in many processes such as film-casting and coating. As for the elongation behavior of a polymeric film, some commercial measurement methods are available. However, these measurement methods cannot be applied to liquids with lower viscosities. A method of measuring planar elongation viscosity, especially for low viscosity liquids, has been proposed, which generates a planar elongation flow by pushing a bullet-shaped bob into a cup filled with the sample liquid. The pushing force, which can be measured by a conventional rheometer, reflects the responses of shear, planar extensional deformation, and buoyancy. However, measurements using a bullet-shaped bob may be strongly affected by the shear flow between the bob and the cup. Therefore, an alternative measurement using a flat disk-shaped bob is proposed, in order to significantly reduce the influence of shear flow. However, such improvements cannot be estimated numerically. In this study, we performed numerical simulations of viscoelastic fluids for both measurement methods to clarify the shear flow effects.

Nomenclature

$\boldsymbol{E}$	[Pa]	elastic stress tensor
F	[N]	applied force
g	[m/s^2]	gravity acceleration
$\boldsymbol{g}$	[m/s^2]	gravity vector
G	[Pa]	relaxation modulus
h	[m]	gap between bob and cup
L	[m]	representative length
p	[Pa]	pressure
Q	[m^3/s]	volume flow rate
R	[m]	radius
S	[m^2]	surface area
$\boldsymbol{S}$	[s^{-1}]	rate of deformation tensor
u, w	[m/s]	velocity in r, z direction
$\boldsymbol{v}$	[m/s]	velocity vector
V_b	[m/s]	bob sliding velocity
α, s	[-]	Giesekus model parameter
$\dot{\gamma}$	[s^{-1}]	shear rate
$\boldsymbol{\delta}$	[-]	unit tensor
$\dot{\varepsilon}$	[s^{-1}]	elongation velocity
η_0	[Pa·s]	zero-shear viscosity
θ	[rad]	radial angle
λ	[s]	relaxation time
ρ	[kg/m^3]	density
$\boldsymbol{\tau}$	[Pa]	extra stress tensor
∇	[m^{-1}]	gradient operator
II_d	[s^{-2}]	second invariant of deformation tensor
III_d	[s^{-3}]	third invariant of deformation tensor

Subscripts and Superscripts

b	bob
c	cup
hd	hydraulic mean depth
m	smallest
M	largest
PE	planar elongation
r, *z*	direction
T	transpose
∇	contravariant convective derivative

1 Introduction

Planar elongation flow of viscoelastic fluids can be observed in film-casting, blow molding, and coating processes, among others. Such processes can be affected by the material response under extensional deformation, which is different from the response under shear deformation. To evaluate the planar elongation behavior of such fluids is important for the design and operation of the processes. However, useful planar elongation viscosity measurements are not available, because it is difficult to generate a steady planar elongation flow field, especially for low viscosity fluids. Sugihara et al. [1] proposed a method of measuring the planar elongation viscosity, which uses the planar elongation flow generated by pushing a bullet-shaped bob into a cup filled with the sample liquid. A commercial stress-controlled rheometer was used to measure the normal force at a given bob speed. The normal force is equivalent to the summation of resistance forces acting on the bob, such as a buoyancy force, pressure, and extra stresses due to the elongation and shear flows. The bullet-shaped bob and cup are precisely manufactured to generate a planar elongation flow at a desired planar elongation rate, as shown in Figure 1. This method is useful for lower viscosity liquids. However, the Trouton ratio of the planar elongation viscosity of the Newtonian fluid was approximately 10^3 times higher than the theoretical value of 4. On the other hand, Sugihara et al. [1] also showed numerical results, such as the streamline and shear rate profiles shown in Figure 2. They pointed out that the resistance force on the bob is dominated by shear flow due to the longer narrow gap between the bob and cup, and it is necessary to reduce the influence of the shear flow for accurate planar elongation viscosity measurements.

To reduce the effect of the shear flow at the gap, a flat disk-shaped bob with a knife-edged rim was proposed [2]. Figure 3 shows a schematic view of the disk-shaped bob. This technique was intended to reduce the influence of the shear flow significantly because the length of the narrow gap is infinitesimally short. However, it was necessary to assume a representative length L of the shear and elongation flow region instead of the length of the test section in order to estimate the resistance force to evaluate the planar elongation viscosity. The choice of this representative length is important to increase the accuracy of the elongation viscosity measurement. They used the hydraulic mean depth as the representative length, so that Trouton ratio of the flow channel of Newtonian fluids agrees with the theoretical value of 4. Ideally, the representative length characterizing the flow field should be determined based on an analytically or experimentally obtained velocity distribution. The flow field occurring around the disk-shaped bob and the cup, however, has not yet been revealed. In this study, we perform a numerical simulation of a viscoelastic fluid for the flat disk-shaped bob to clarify the effect of the shear flow region on the resistance force and the validity of using the hydraulic mean depth as the representative length.

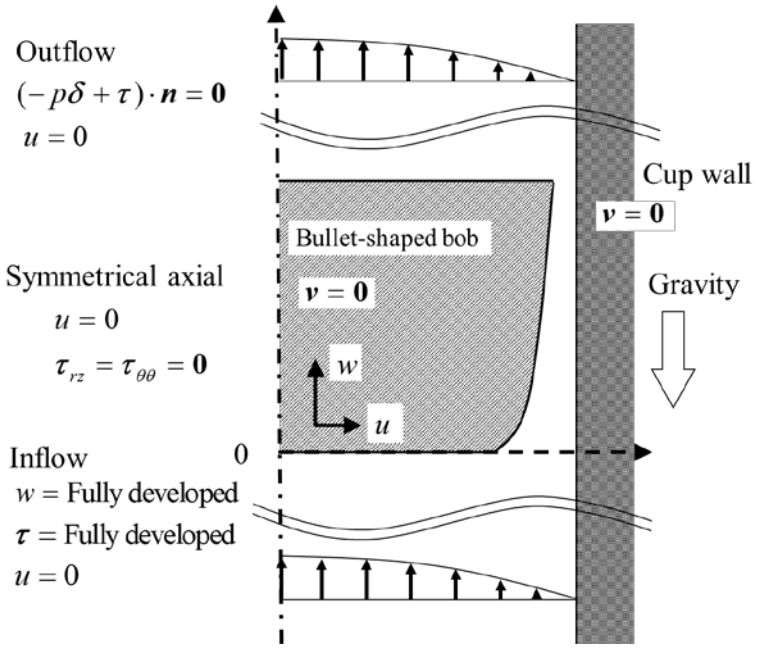

Figure 1. Boundary conditions of flow analysis in the bullet-shaped bob geometry.

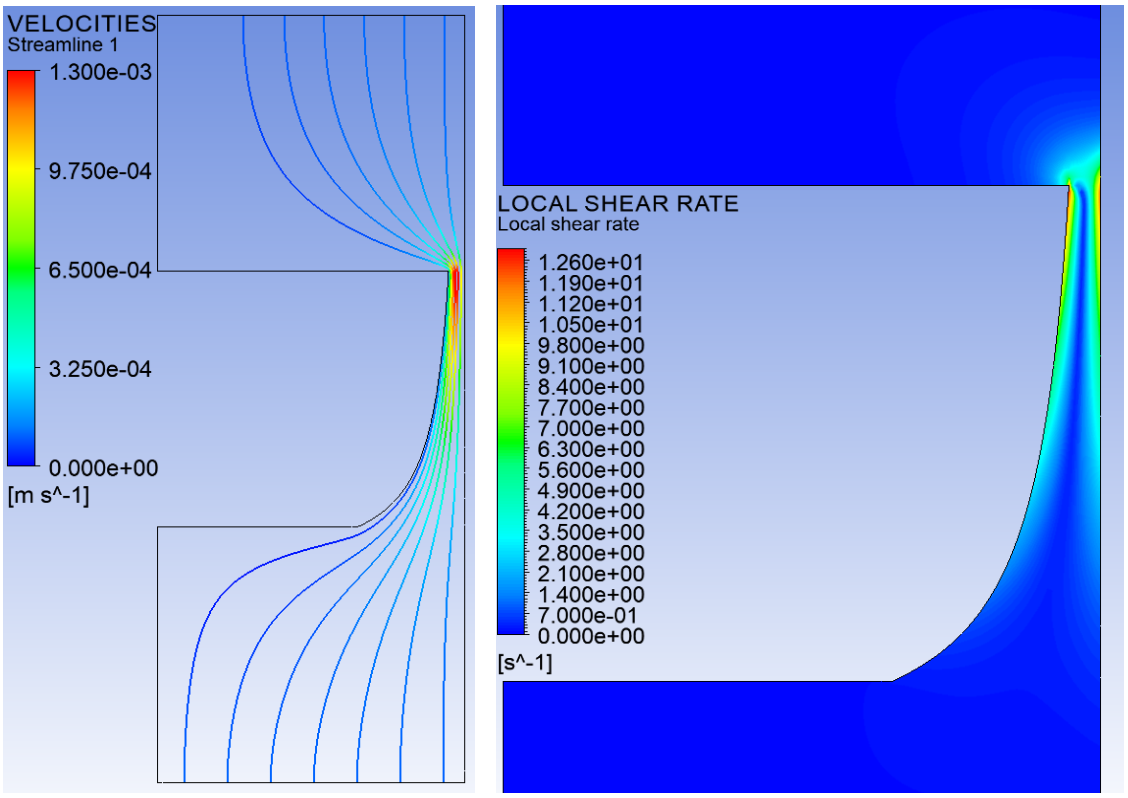

Figure 2. (a) Streamlines and velocity profile and (b) shear rate profile of the flow channel between the cup and bullet-shaped bob sliding at V_b=0.1 mm/s.

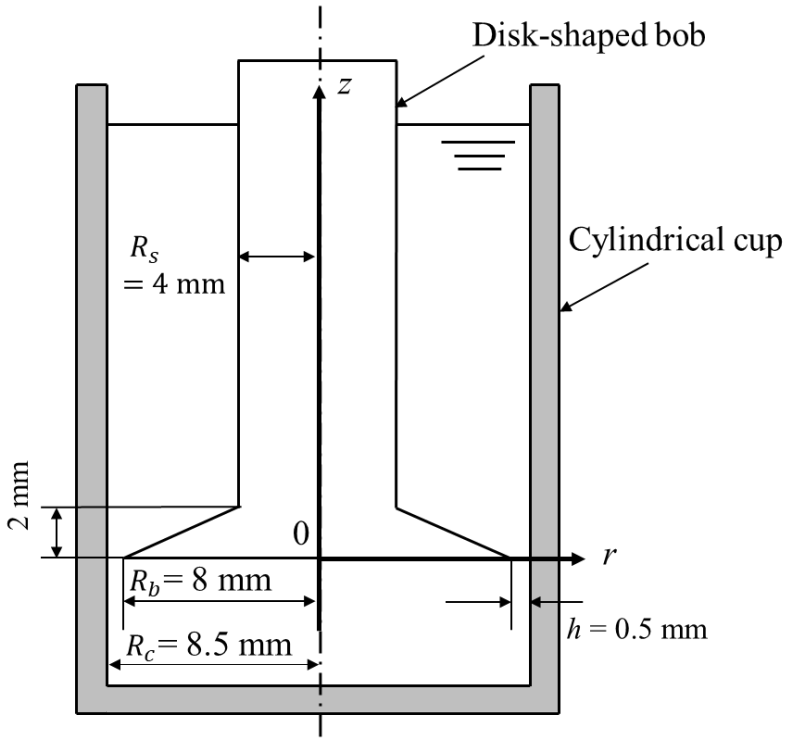

Figure 3. Schematic of flow problem between the disk-shaped bob and cylindrical cup.

2 Numerical Analysis

2.1 Governing Equations

The isothermal and steady state flow of a viscoelastic fluid is governed by the following basic equations, i.e., equation of continuity (1), momentum equation (2) and constitutive equations (3) and (4) as follows.

$$\nabla \cdot \boldsymbol{v} = 0 \tag{1}$$

$$\rho \boldsymbol{v} \cdot \nabla \boldsymbol{v} = -\nabla p + \nabla \cdot \boldsymbol{\tau} + \rho \boldsymbol{g} \tag{2}$$

$$\boldsymbol{\tau} = 2\eta_0 s \boldsymbol{S} + \boldsymbol{E} \tag{3}$$

$$\boldsymbol{E} + \lambda \overset{\triangledown}{\boldsymbol{E}} + (\alpha / G)\boldsymbol{E}^2 = 2\eta_0 (1-s)\boldsymbol{S} \tag{4}$$

where $\boldsymbol{S}$ is the deformation tensor ($2\boldsymbol{S} \equiv \nabla \boldsymbol{v} + \nabla \boldsymbol{v}^{\mathrm{T}}$) and the upper convected derivative of the elastic stress $\overset{\triangledown}{\boldsymbol{E}}$ defined in equation (5), which is the elastic part of the extra stress $\boldsymbol{\tau}$. The unit mode Giesekus model [3] is employed as a constitutive equation with a zero-shear viscosity η_0, a relaxation time λ, model parameters α, s and relaxation modulus $G \equiv \eta_0 (1-s)/\lambda$.

$$\overset{\triangledown}{\boldsymbol{E}} \equiv \boldsymbol{v} \cdot \nabla \boldsymbol{E} - (\nabla \boldsymbol{v}^{\mathrm{T}} \cdot \boldsymbol{E} + \boldsymbol{E} \cdot \boldsymbol{v}) \tag{5}$$

The elastic–viscous–split–stress (EVSS) method [4] for viscoelastic flows is used to improve the convergence of the analysis. Biquadratic interpolation and linear interpolation are used for the velocity and the pressure field, respectively. A 4×4 sub element scheme and stream up winding method [5] are employed for discretization of constitutive equations using the Galerkin finite element method by POLYFLOW software ANSYS 19.0.

2.2 Boundary Conditions

Figure 3 is a schematic illustration of the flow geometry with a disk-shaped bob. 2D asymmetrical flow was assumed in this simulation. The radius of the disk-shaped bob, the rod, and the inner cup are R_b, R_s, and R_c, respectively. The upper part of the disk is slightly conical in shape.

Boundary conditions are summarized in Figure 4. The flow at the inlet boundary is taken to be fully developed at a given flow rate with a specified profile velocity and components of the elastic stress $\boldsymbol{E}$, as well as the total stress are set to vanish at the outlet. No-slip conditions are assumed along the surfaces of the cup wall and the bob. The bob is fixed, and the cup wall moves up at the bob sliding speed V_b.

Figure 5 shows a mesh profile of the calculation domain consisting of 7,620 elements. A close-up of the mesh profile around the tip of the disk-shaped bob is shown on the right side. The tip of the disk-shaped bob is slightly rounded to relax the singularity effect.

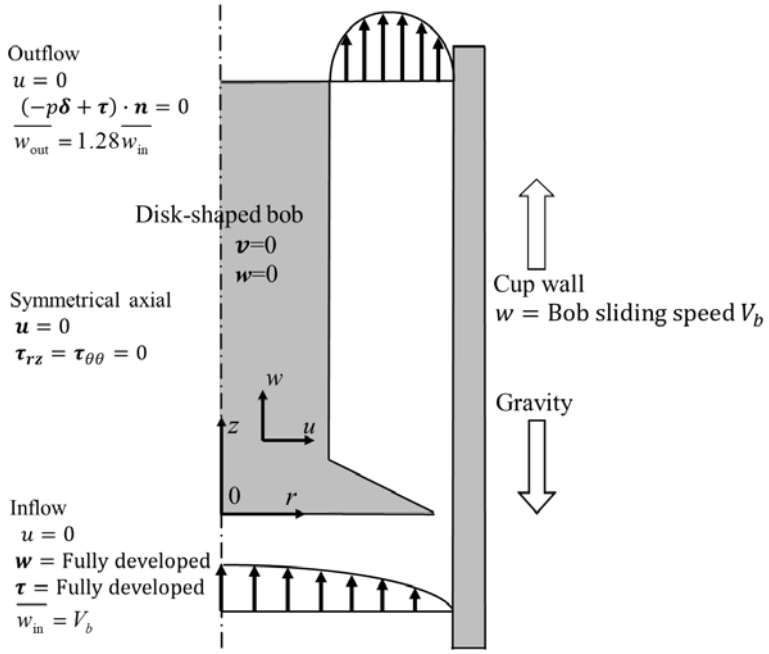

Figure 4. Boundary conditions for flow analysis between the cup and disk-shaped bob.

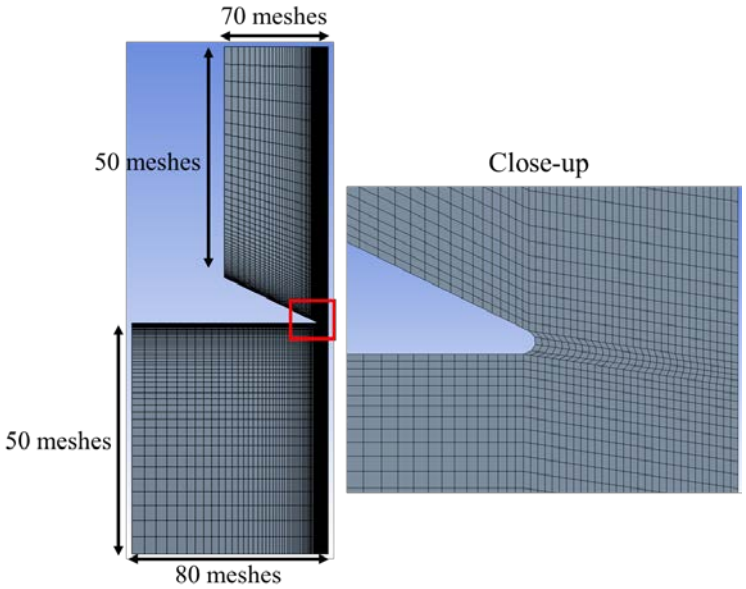

Figure 5. Overview of mesh profile (left side) and its close-up view around the tip of the disk (right side).

2.3 Material

M1 fluid [7, 8] was used as a low-viscosity viscoelastic liquid, and was measured by a rheometer MCR301 (Anton Paar Corp.). Figure 6 shows the rheological properties of the M1 fluid. The M1 fluid shows an almost constant shear viscosity over the tested shear range but exhibits slightly shear-thinning behavior (Figure 6). The data of storage modulus *G'* and loss modulus *G"* are replotted from Te Nijenhuis et al. [10].

We also fit parameters of the unit mode Giesekus model to the experimental data. The rheological curves obtained by this fitting are shown as the solid lines in Figure 6. The model parameters used in the simulations are η_0 = 1.64 Pa·s, λ = 0.200 s, α = 0.500, and s = 0.595.

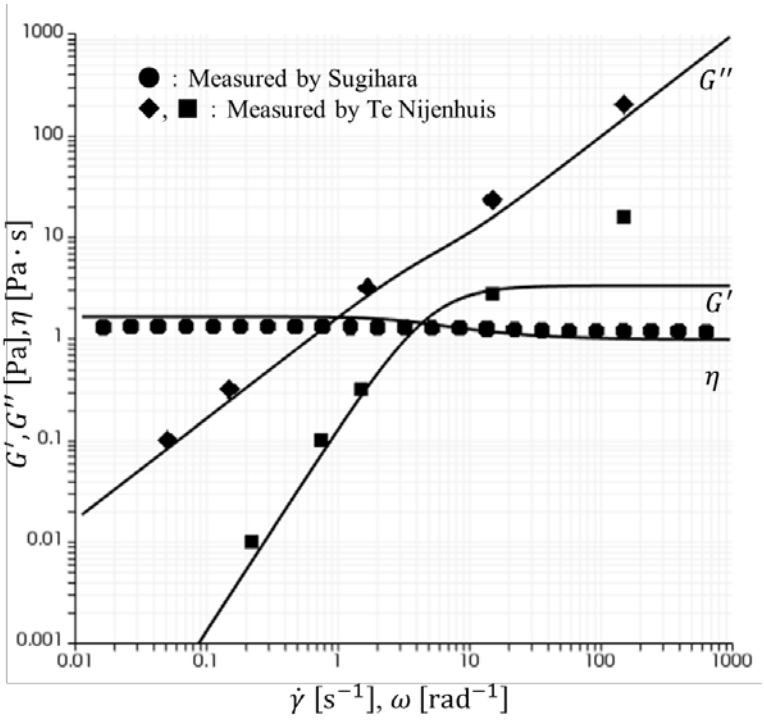

Figure 6. Rheological properties of the M1 fluid: Storage modulus *G'*, Loss modulus *G"*, Shear viscosity η.

2.4. Estimation of Resistance Forces

In the case of the disk-shaped bob, the summation of the apparent resistance force *F'* can be written as:

$$F' = F - F_b = F_{ss} + F_{sn} + F_{PE} \tag{6}$$

where F is the net resistance force, F_b is the buoyancy force, F_{ss} is the contribution of the shear stress acting on the aspect of the bob, F_{sn} is the contribution of the pressure drops of the shear flow, and F_{PE} is generated by the planar elongation flow in the test section [2]. In the case of the bullet-shaped bob, F_{sn} will be the dominant force, because the shear stress acting on the bullet-shaped bob is much bigger due to the longer channel, as shown in Figure 2(a). However, the shear stress acting on the surface of the disk-shaped bob can be neglected because of the knife-edged rim, giving F_{ss}=0. In addition, shear stress will be generated on the cup surface in the narrow gap region. Sugihara et al. [2] assumed that F_{sn} is given as follows:

$$F_{sn} = \pi R_b^2 \int_0^L \left(-\frac{dp}{dz}\right) dz = \pi R_b^2 \left(-\frac{dp}{dz}\right) L \tag{7}$$

In the experimental measurement of planar elongation, we treat the M1 fluid as a power-law fluid (flow coefficient power-law index K=1.25 Pa·s^n) [2]. Assuming a power-law fluid, the pressure gradient over a representative length L can be calculated. Finally, the planar elongation rate can be given as follows:

$$\dot{\varepsilon}_{PE} = \frac{Q}{\pi\left(R_c^{\,2} - R_b^{\,2}\right)} \times \frac{1}{L} = \frac{R_c^{\,2} V}{L\left(R_c^{\,2} - R_b^{\,2}\right)} \tag{8}$$

Here, the choice of representative length L is important for the disk-shaped bob. Sugihara et al. [2] used the hydraulic mean depth L_{hd} as L [9], which gave the experimentally obtained Trouton ratio of the Newtonian fluid the theoretically predicted value of 4.

$$L_{hd} = \frac{\pi\left(R_c^{\,2} - R_b^{\,2}\right)}{2\pi\left(R_c + R_b\right)} = \frac{R_c - R_b}{2} \tag{9}$$

L_{hd} is half of the width between the tip of the disk-shaped bob and the cup wall.

3 Results and Discussion

3.1 Results of Numerical Simulation

Figure 7 shows the apparent resistance force F' generated by the flow between the cup and the bob. The solid line with open circles indicates experimental values replotted from [2]. The dashed line with solid circles indicates F' obtained by the numerical simulation. F' increases linearly and agrees well with the experimental data. The relative error with respect to the experimental value at V_b=10 mm/s is -0.73%. Therefore, the validity of the numerical simulation is confirmed.

Figure 8(a) shows streamlines in the flow field. The magnitude of velocity is indicated on each streamline by the color scale. Fully developed flow enters from the bottom of the cup. The mean inlet velocity in the z-direction $\overline{w_{in}}$ is 0.1 mm/s, which is the same as the bob sliding velocity V_b. The streamlines are parallel to each other. The streamlines are gradually concentrated and smoothly enter the narrow gap between the disk-shaped bob and cup. However, no vortex was found in the calculation domain. Approaching the gap from the bottom, the flow velocity is dramatically increased up to about 8.76 times faster than the mean inlet velocity. The value is dependent on the flow geometry. After passing through the narrow gap, the streamlines diverge smoothly and the velocity profile changes again to parallel flow. Numerical results at V_b = 10 mm/s are similar to those at V_b = 0.1 mm/s.
Figure 8(b) shows a contour plot of the elongation rate, which can be evaluated by equation (10) [6],

$$\dot{\varepsilon}_{PE} = 3III_d \,/\, II_d \tag{10}$$

where II_d and III_d are the second and third invariants of the deformation tensor $\boldsymbol{S}$, respectively. It was found that strong elongation flow is clearly generated in the entrance region of the narrow gap.

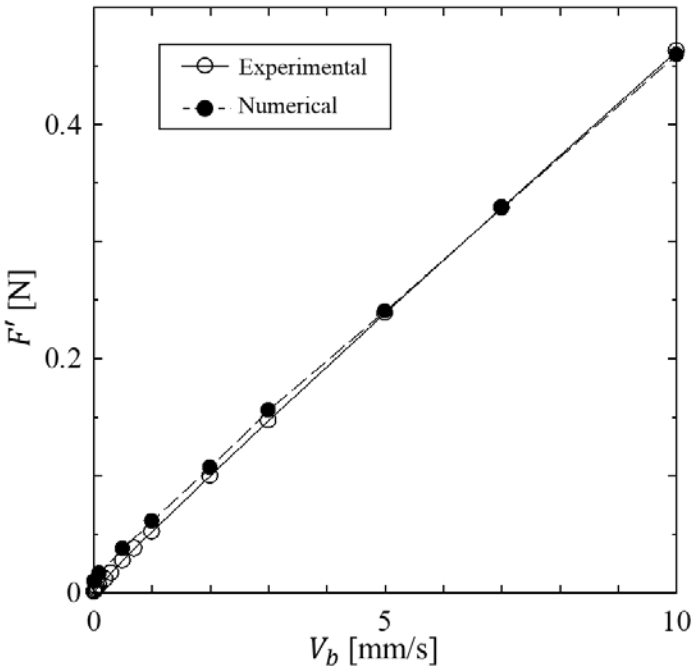

Figure 7. Apparent resistance force generated by flow between the cup and the bob.

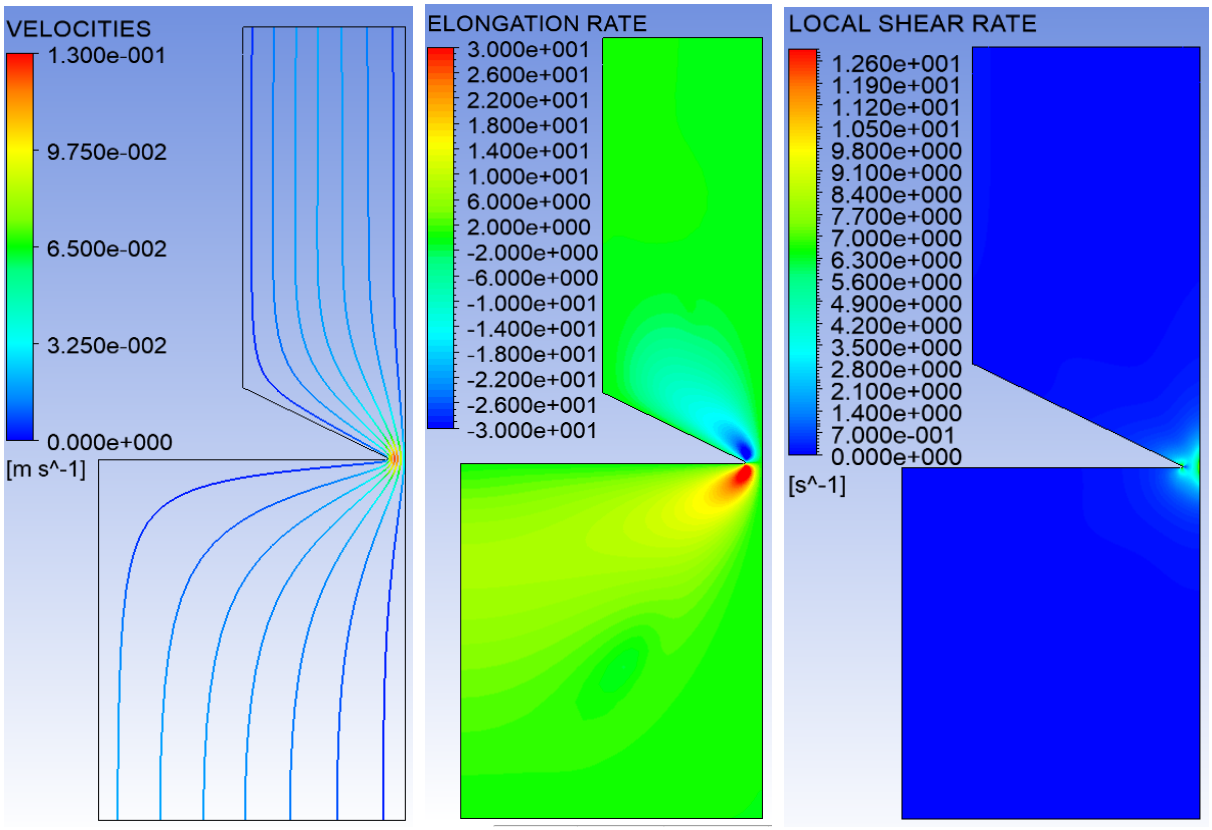

Figure 8. (a) Streamlines and velocity profile of the M1 fluid. Sliding velocity of the disk-shaped bob was V_b=0.1 mm/s. (b) Elongation rate profile at V_b=0.1 mm/s. (c) Shear rate profile at V_b=0.1 mm/s.

3.2 Validity of Representative Length

A shear rate profile for the calculation domain is given in Figure 8(c). It is readily apparent that the area of shear flow in the disk-shaped geometry is much smaller than in the bullet-shaped bob geometry shown in Figure 2(b).

An enlarged view of the shear rate contour plot around the edge of the disk is shown in Figure 9. The wall shear on the cup is biggest just beside the tip and falls off rapidly with increasing distance from the tip. Figure 10 shows the normalized wall shear rate along the cup surface near the tip. The shear rates at four sliding speeds (V_b=0.1, 1, 5, 10 mm/s) were normalized by the maximum value. The lines are very similar in shape near the tip. This means that the normalized shear region is independent from the bob sliding velocity V_b. Therefore, it is reasonable to determine the representative length from the shear rate profile on the cap wall. The hydraulic mean depth L_{hd} matches the range of high shear rate, $\dot{\gamma}/\dot{\gamma}_{\max} \geq 0.9$. Thus, the assumption of representative length is reasonable in the estimation of elongation viscosity.

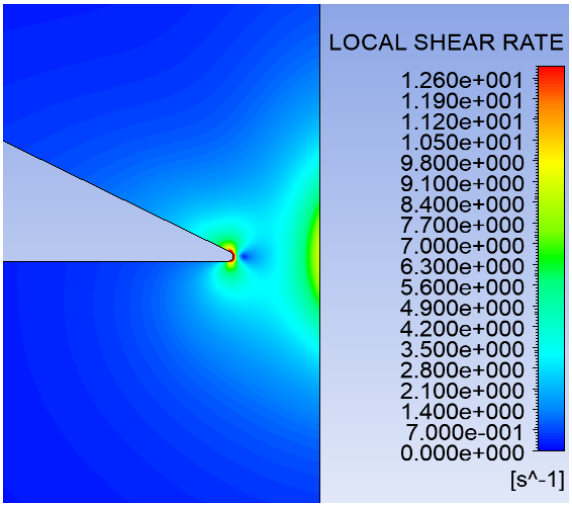

Figure 9. Shear rate profile around the edge of a disk-shaped bob at V_b=0.1 mm/s.

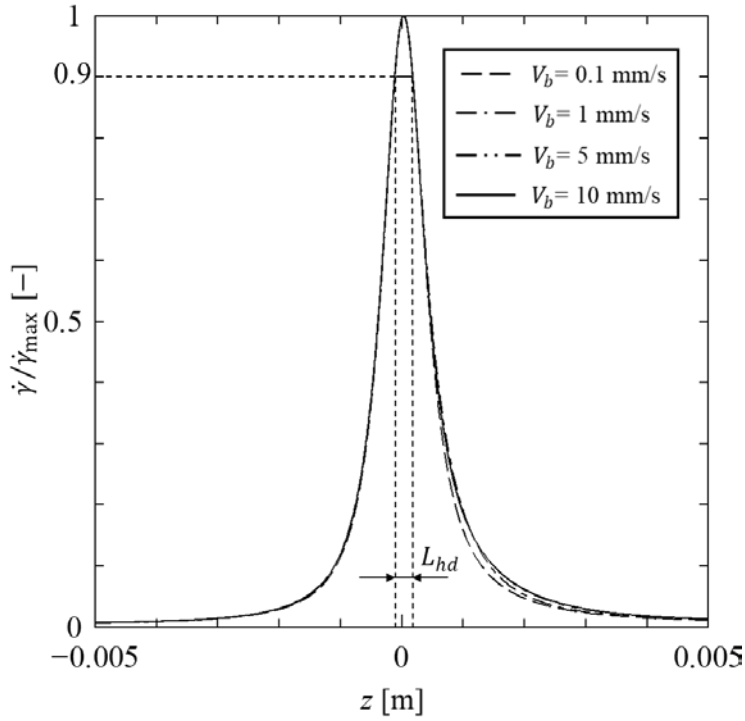

Figure 10. Effect of bob velocity V_b on normalized shear rate on the cup wall surface. R_b=8 mm, R_c=8.5 mm, h=0.5 mm, L_{hd}=0.25 mm.

3.3 Effect of Bob Geometry on Representative Length

We examined the effect of the radius and gap geometry on the shear rate profile along the cup wall. The bob geometry was changed gradually in two ways: (1) R_c and R_b were changed with constant gap h, and (2) the gap h between the bob and cup was changed with constant cup radius R_c. Figure 11 shows the calculation results for the constant gap cases. The shear rate on the cup wall is normalized by its maximum value. Twenty lines overlap in Figure 11, and they are all very similar to each other near the tip. Each hydraulic mean depth L_{hd} agrees with the range of over 90% of its maximum shear rate value.

Figure 12 shows the simulations result for the constant R_c cases. The bob radii are varied as R_b=6.5, 7.5, 8, 8.1 mm, and the gaps are varied as h=2, 1, 0.5, 0.4 mm. The shear rate on the cup wall is normalized by its maximum value. When the horizontal axis of the figure is normalized by the gap h, the similar profiles were obtained. These simulation results indicate that the choice of L_{hd} is applicable to various bob geometries.

R_b [mm]	R_c [mm]	h [mm]
8	8.5	0.5
5	5.5	0.5
11	11.5	0.5
20	20.5	0.5
25	25.5	0.5
8.1	8.5	0.4
7.5	8.5	1
6.5	8.5	2

Table 1. Geometric parameters of the disk-shaped bob.

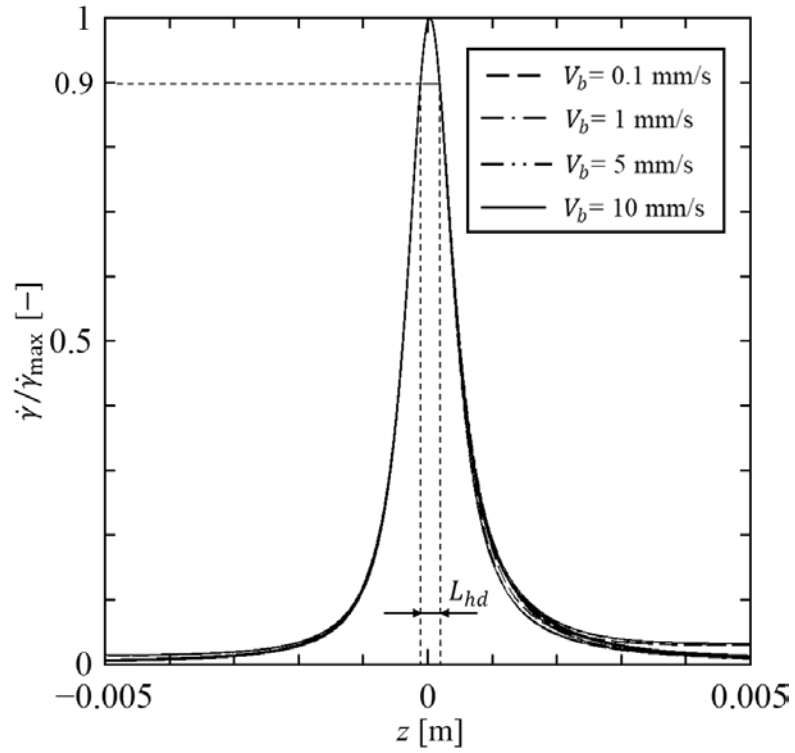

Figure 11. Normalized shear rate on cup wall surface near the tip. R_b=5, 8, 11, 20, 25 mm. L_{hd}=0.25 mm.

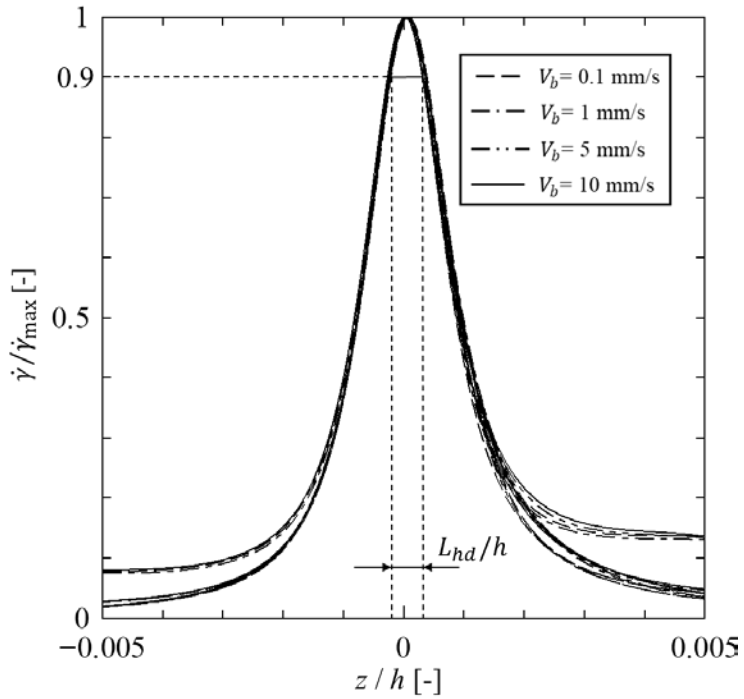

Figure 12. Normalized shear rate on cup wall surface near the tip. R_b=6.5, 7.5, 8, 8.1 mm. L_{hd}/h=0.5 mm.

3.4 Effect of Thickness of the Disk-shaped Bob on Resistance Force

The accuracy of the estimation of planar elongation viscosity can be improved by increasing the contribution of the planar elongation stress F_{PE} compared to the resistance force F'. In the case of the bullet-shaped bob, the ratio of F_{PE} to F' is about 0.4% [1] due to the bigger shear region as shown in Figure 2(b). However, in the case of the disk-shaped bob, the ratio can be dramatically improved up to 44.8% at V_b=10 mm/s, because the region of shear flow near the narrow gap is eliminated. We numerically evaluated the effect of the longitudinal length (bob thickness l) of the narrow gap, as shown in Figure 13, on the ratio of F_{PE} to F'.

Figure 14(a) shows streamlines in the flow field at l=5 mm and V_b=0.1 mm/s. Figure 14(b) shows a contour plot of the elongation rate. The maximum elongation rate is almost the same as that at l=0 mm and V_b=0.1 mm/s. A shear rate profile for the calculation domain is shown in Figure 14(c). Strong shear flow is obvious in the narrow gap region depending on the length of l and that increases the shear contribution, F_{ss} and F_{sn}. Figure 15 shows the effect of the thickness length l and the bob sliding speed V_b on the apparent resistance force F'. The numbers on the right side indicate the ratio of the elongation stress term F_{PE} to the apparent resistance force F' at V_b=10 mm/s. It is clear that the thinner disk-shaped bob is preferable for the measurement of elongation viscosity.

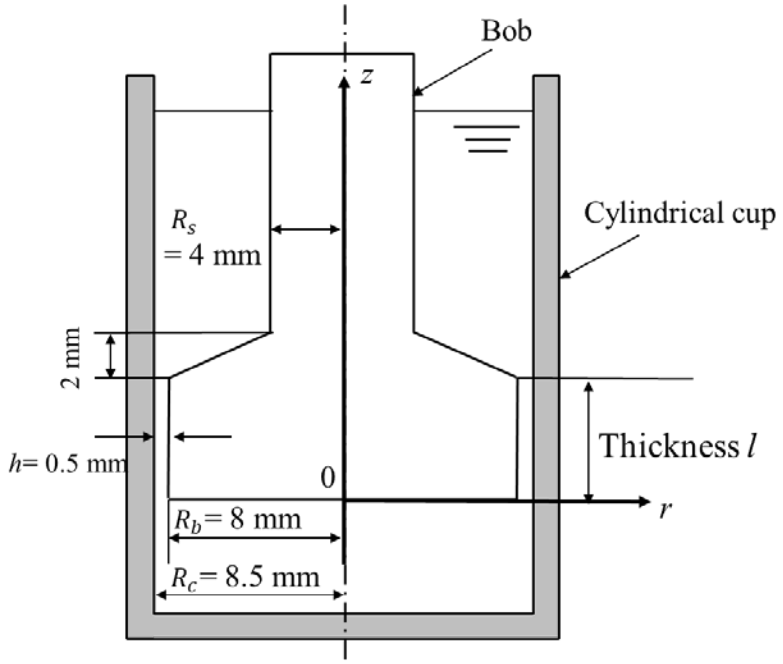

Figure 13. Schematic of flow with a disk-shaped bob and a cylindrical cup. The disk-shaped bob has thickness *l*.

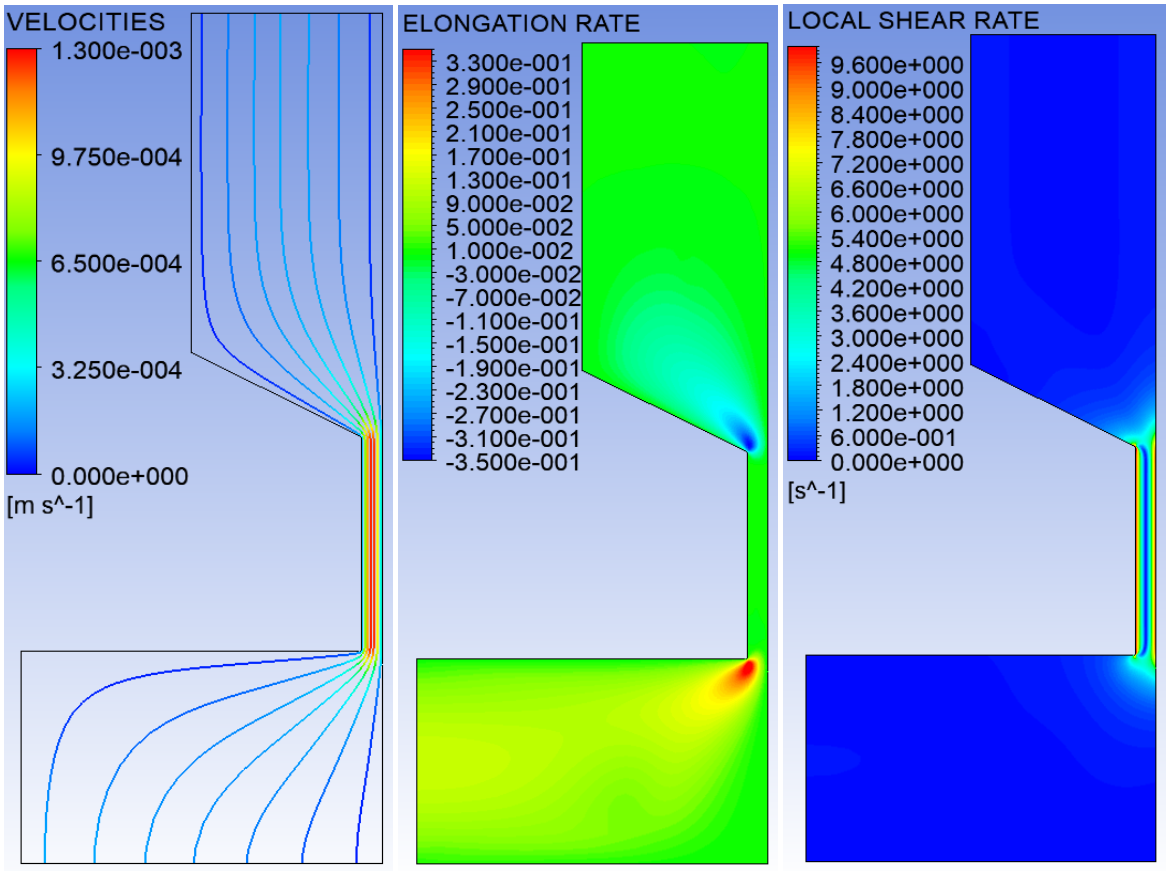

Figure 14 (a). Streamlines and velocity profile of the M1 fluid. Thickness of the disk-shaped bob is l=5 mm. Sliding velocity of the disk-shaped bob is V_b=0.1 mm/s, (b) Elongation rate distribution. l=5 mm, V_b=0.1 mm/s, (c) Shear rate distribution. l=5 mm, V_b=0.1 mm/s.

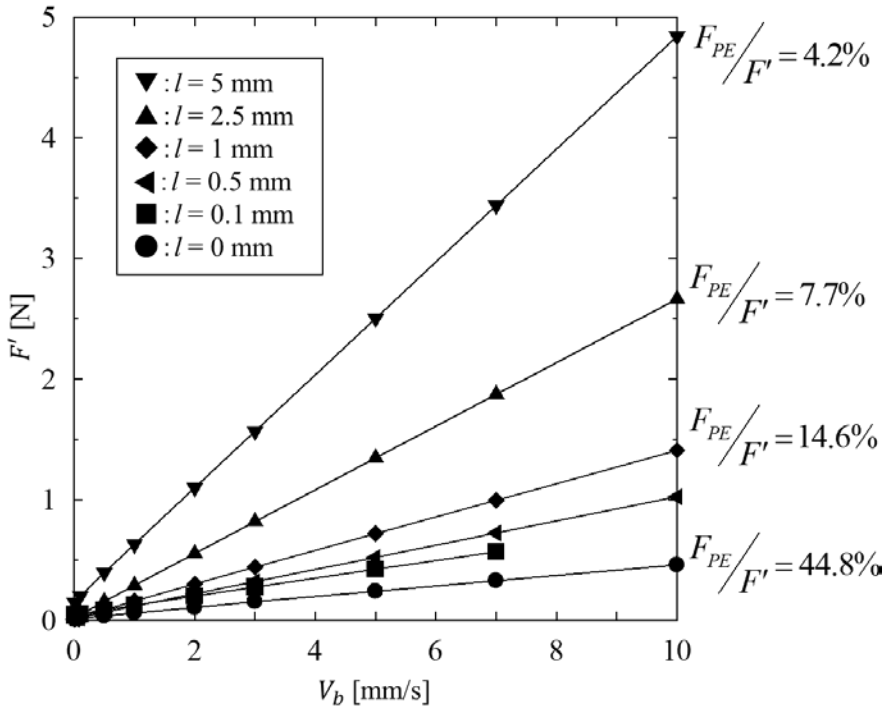

Figure 15. Apparent resistance force generated by flow between the cup and the bob. Left numbers indicate the contribution of planar elongation at a bob velocity V_b of 10 mm/s.

Conclusions

We performed a numerical simulation of a viscoelastic fluid for the measurement method using a disk-shaped bob developed by Sugihara et al. [2]. Approaching the gap, flow velocity increases dramatically, and a strong elongation velocity is clearly generated in the entrance region of the narrow gap.

The wall shear rate profiles near the tip are similar for four different bob sliding speeds. The width of the normalized strong shear region was the almost same as the hydraulic mean depth. Therefore, the validity of this assumption in the calculation of elongation viscosity for the disk-shaped bob was confirmed.

The effects of bob and cup geometry were examined. The hydraulic mean depth matched the region of high wall shear rate, confirming the validity of the use of the hydraulic mean depth as the representative length.

Shear rate distributions for the disk-shaped bob and the bullet-shaped bob are compared. The effect of shear in the disk-shaped geometry is much smaller than that in the bullet-shaped bob. The thinner disk-shaped bob is preferable for the measurement of elongation viscosity, because the influence of shear flow along the wall surface is significantly reduced.

Acknowledgements

The authors would like to thank Ms. Akiko Onishi and Mr. Wataru Kubota for technical assistance with the experiments. This work was supported by JSPS KAKENHI Grant Numbers (No. 17K06152) from the Japan Society for the Promotion of Science (JSPS).

References

[1] Sugihara, Y.; Kubota, W.; Yoshitake, Y.; Takahashi, T.; Iwata, S.; Nagumo, R.; and Mori, H.: Development of Mechanical Measurement Technique for Planar Elongation Viscosity Using Resistance Force on Pushing Bullet Bob. *Nihon Reoroji Gakkaishi*, 44, (2016), 175-183.

[2] Sugihara, Y.; Iwata, S.; and Takahashi T.: Evaluation of planar elongation viscosity of low-viscosity liquids using annular abrupt contraction flow around a sliding disk-shaped bob. *Rheologica Acta*, 57, (2018), 97-104.
[3] Giesekus, H.: A Simple Constitutive Equation for Polymer Fluids Based on the Concept of Deformation-Dependent Tensorial Mobility. *J. Non-Newtonian Fluid Mech.*, 11, (1982), 69-109.
[4] Rajagopalan, D.; Armstrong, R.; and Brown, R.: Finite element methods for calculation of steady, viscoelastic flow using constitutive equations with a Newtonian viscosity. *J. Non-Newtonian Fluid Mech.*, 36, (1990) 159-192.
[5] Marchal, J. M.; and Crochet, M. J.: A new mixed finite element for calculating viscoelastic flow. *J. Non-Newtonian Fluid Mech.*, 26, (1987), 77-113.
[6] Debbaut, B.; and Crochet, M. J.: Extensional effects in complex flows. *J. Non-Newtonian Fluid Mech.*, 30, (1988), 169-184.
[7] Nguyen, D. A.; and Sridhar, T.: Preparation and some properties of M1 and its constituents. *J. Non-Newtonian Fluid Mech.*, 35, (1990), 93-104.
[8] Binding, D. M.; Jones D. M.; and Walters, K.: The shear and elongation flow properties of M1. *J. Non-Newtonian Fluid Mech.*, 56, (1990), 121-135.
[9] Ushida, A.; Kawami, M.; Uchiyama, H.; Narumi, T.; Kayaba, R.: Flow properties of microbubble/polyethylene glycol mixtures passing through orifices and slits. *Nihon Reoroji Gakkaishi*, 40, (2012), 61-68.
[10] Te Nijenhuis, K.; Van Benschop, H. J.: Glass transition temperature, specific gravity, viscosity and viscoelastic properties of the test fluid M1. *J. Non-Newtonian Fluid Mech.*, 35, (1990), 179-187.

Addresses: Shunsaku Ito, Department of Life-Science and Applied Chemistry, Graduate School of Engineering, Nagoya Institute of Technology, Gokiso-cho, Showa-ku, Nagoya, Aichi 466-8555, Japan. email: ito.shunsaku@chemeng.nitech.ac.jp
Prof. Dr. Shuichi Iwata, Department of Life-Science and Applied Chemistry, Graduate School of Engineering, Nagoya Institute of Technology, Gokiso-cho, Showa-ku, Nagoya, Aichi 466-8555, Japan. email: iwa@nitech.ac.jp
Dr. Yukinobu Sugihara, Department of Electronic Control Engineering, National Institute of Technology, Nagaoka College, 888 Nishikatakai, Nagaoka, Niigata 940-8532, Japan. email: ysugi@nagaoka-ct.ac.jp
Prof. Dr. Tsutomu Takahashi, Department of Mechanical Engineering, Nagaoka University of Technology, 1603-1, Kamitomioka Nagaoka, Niigata 940-2188, Japan. email: ttaka@nagaokaut.ac.jp